

Research Article

Open Access



Improving the pore properties of porous aromatic frameworks in two aspects via partition strategy

Hengtao Lei, Zhaofu Zhang, Yuhui Zhai, Xueyan Han, Jian Song, Yue Li*, Yuyang Tian*

Key Laboratory of Polyoxometalate and Reticular Material Chemistry of Ministry of Education, Faculty of Chemistry, Northeast Normal University, Changchun 130024, Jilin, China.

*Correspondence to: Prof. Yuyang Tian, Dr. Yue Li, Key Laboratory of Polyoxometalate and Reticular Material Chemistry of Ministry of Education, Faculty of Chemistry, Northeast Normal University, 5268 Renmin Street, Changchun 130024, Jilin, China. E-mail: tianyy100@nenu.edu.cn; liy225@nenu.edu.cn

How to cite this article: Lei H, Zhang Z, Zhai Y, Han X, Song J, Li Y, Tian Y. Improving the pore properties of porous aromatic frameworks in two aspects via partition strategy. *Chem Synth* 2024;4:62. <https://dx.doi.org/10.20517/cs.2024.16>

Received: 2 Feb 2024 **First Decision:** 24 May 2024 **Revised:** 19 Jun 2024 **Accepted:** 27 Jun 2024 **Published:** 15 Oct 2024

Academic Editor: Wei Li **Copy Editor:** Pei-Yun Wang **Production Editor:** Pei-Yun Wang

Abstract

Microporous solids are famous for their high surface area and pore size at the molecular scale, which are crucial for the applications of adsorption, separation and catalysis. An ideal porous solid would simultaneously have a high surface area and nanopores with the desired opening size. However, due to the uncontrollable reaction process of porous organic frameworks (POFs), the acquisition of such a solid is still technically limited. Herein, we reported a simple but platform-wide pore partition strategy to improve the porosity of porous aromatic frameworks (PAFs) in two aspects. This strategy was achieved by introducing a partition unit with flexible linkage to segment the original voids of PAFs into multiple micropore domains. The obtained partitioning PAFs have 130%-217% increments in surface area due to the creation of extra accessible surfaces while the pores are segmented into smaller ones. Notably, the partitioning PAFs showed significantly increased adsorption capacity for CO₂ due to their improved surface area. At the same time, the narrowed pore size allowed selective capture of dye molecules by their size differences. Similar to their parent PAFs, the partitioning PAFs retained their high stability in harsh environments. A simple and universal pore partition strategy will be an important step in improving PAF porosity to desired functions.

Keywords: Porous aromatic frameworks, pore partition strategy, size-dependent adsorption



© The Author(s) 2024. **Open Access** This article is licensed under a Creative Commons Attribution 4.0 International License (<https://creativecommons.org/licenses/by/4.0/>), which permits unrestricted use, sharing, adaptation, distribution and reproduction in any medium or format, for any purpose, even commercially, as long as you give appropriate credit to the original author(s) and the source, provide a link to the Creative Commons license, and indicate if changes were made.



INTRODUCTION

Porous solids, such as zeolites^[1,2], metal-organic frameworks (MOFs)^[3,4] and porous organic frameworks (POFs)^[5-7], have lately attracted considerable attention and offered a lot of application prospects in various fields, including gas adsorption and storage^[8-10], size-dependent molecule recognition^[11-13], sensing^[14,15], proton conduction^[16,17], heterogeneous catalysis^[18-20], and so on^[21,22]. POFs are significantly attractive for these applications because of their diverse chemical properties^[23,24], controllable pore functions^[25], and exciting stability^[18]. Surface area and pore size are two crucial features for the performance of POFs and other porous solids. A large surface area introduces as much exposed accessible surface, significantly improving the catalytic activity and adsorption capacity of the framework^[26,27]. For pore size, size-dependent molecular recognition highly depends on the size and shape of the micropores. Once within the corresponding size range, an ideal porous material, or at least a portion of the pores, can only accommodate smaller molecules while completely blocking larger ones^[28-30]. For example, Lin *et al.* used rigid square acid and calcium nitrate to limit the pore size to 3.8 Å, achieving the separation of C₂H₄ and C₂H₆^[31]. Therefore, at the molecular level, high surface area and well-controlled pore size are of great significance for the synthesis and regulation of POFs.

In recent years, pore-partition strategy for tuning the pore space has received extensive attention^[32]. A representative example of pore partition is a prototype of partitioned aces (pacs). An ace-type (MOF-235) framework formed by metal trimers and ditopic ligands was partitioned into small pores by a pore partition agent^[33,34]. In addition, the POFs with various anchoring groups in their frameworks by functional building units were synthesized, and these anchored groups can be further quantitatively reacted to introduce additional functional units to segment pore space^[35,36]. Xu *et al.* were able to segment a mesoporous boroxine covalent organic framework (COF) with a fixed pore size of 2.9 nm into six microporous domains with a size of 0.65 nm using a pore partition strategy^[35]. Moreover, Hao *et al.* divided tetragonal or hexagonal pores into two or three smaller micropores, respectively, by inserting additional symmetric building blocks with aldehyde groups anchored in multivariate COF pores^[36]. However, the parent framework must pre-quantitatively anchor functional groups as reaction sites in advance, which increases the difficulty for the parent framework synthesis. The pore size and pore partition agent must meet the requirements of position symmetry and size matching, which imposes higher requirements for the selection of the pore partition agents. Additionally, the surface area of most frameworks has decreased to certain degrees after pore partition. It is still challenging to apply the pore partition strategy to narrowing the existing pores while increasing the surface area of the framework.

Porous aromatic frameworks (PAFs) represent an important category of POFs. They have rigid backbones constructed from organic building units through irreversible cross-coupling reactions, which created strong carbon-carbon covalent bonds, making them tolerant of harsh environments^[37,38]. The irreversibility of the connecting reaction makes the framework kinetically controlled, which leads to amorphous frameworks. The amenability of PAFs and their exceptional stability render them excellent size tolerance for matching pore partition agents. In 2021, Liu *et al.* reported a method of post-knitting conjugated microporous polymers (CMPs) by using external cross-linkers to increase the surface area of the material^[39]. The Friedel-Crafts reaction catalyzed by Lewis acid in this work has an accessible range of reaction sites and flexible crosslinking agents. Overall, we suggest that the flexibility of a partition agent will provide high dimensional tolerance when a strict requirement on position and size match between the parent frameworks and the pore partition agent is necessary. The Friedel-Crafts alkylation reaction introduces a benzyl chloride-containing unit to flexible and carbon-carbon bonded in the framework, which was selected as a pore partition method for pore partition^[40,41]. Meanwhile, the benzene ring backbones of PAFs provide high-density reaction sites. It is expected to become a candidate to meet the requirements, achieving flexible

connections to partition the pores and construct extra accessible surfaces.

Herein, a pore partition strategy was adopted to improve the porosity of PAFs, and 4,4'-bis(chloromethyl)-1,1'-biphenyl (PCBP) with node flexibility was selected as the pore partition agent. The Friedel-Crafts alkylation reaction could be carried out without modification, allowing the original voids to be segmented into multiple micropore domains and construct an extra accessible surface to increase the surface area of PAFs. PAF-11 and PAF-140, synthesized by Suzuki-Miyaura coupling and Sonogashira-Hagihara coupling, respectively, were utilized as parent frameworks. The results indicated that this pore partition strategy could adjust the porosity of the PAFs in two aspects. Compared to the parent PAFs, the surface area of the partitioning PAFs increased more than $1,000 \text{ m}^2 \cdot \text{g}^{-1}$, which is in a ratio of 130%-217%. Consequently, we further examined the CO_2 adsorption performance of the partitioning PAFs, which showed improvement compared to the parent PAFs. The original voids of the parent PAFs were also segmented from 4.1, 2.3 and 1.3 nm to the microporous sizes of 1.1 and 0.5 nm. The micropore volume increased to 192%-275% compared to the parent framework. Through adsorption experiments on dye molecules of different sizes, it was found that the parent PAFs had good adsorption for large-sized dye molecules. In contrast, the partitioning PAFs exhibited a higher adsorption capacity for small-sized dye molecules.

EXPERIMENTAL

Materials and chemicals

All the reagents and anhydrous solvents of analytical purity were purchased from commercial sources without further purification. All the characterization instruments are listed in the [Supplementary Materials](#) without other information [[Supplementary Section 1](#)]. PAF-11 was synthesized according to a previously reported procedure^[42].

Synthesis of parent PAFs

The amount of chemicals required for PAF synthesis is listed in [Supplementary Section 2](#).

Synthesis of PAF-11

PAF-11 was synthesized via Suzuki-Miyaura coupling using tetra(4-bromophenyl)methane (TBPM), 4,4'-biphenyldiboronic acid (BDA), potassium carbonate (K_2CO_3), and tetrakis(triphenylphosphine) palladium (0) refluxed in a solvent of N, N'-dimethylformamide (DMF) at 150 °C for 24 h. After cooling to room temperature, the product was filtered and washed with DMF, H_2O , tetrahydrofuran (THF) and EtOH to remove the catalyst and unreacted monomers. Lastly, the product was dried under vacuum at 100 °C for 8 h to yield off-white powder.

Synthesis of PAF-140

PAF-140 was synthesized via Sonogashira-Hagihara coupling using TBPM, 1,4-diethynylbenzene (DEB), tetrakis(triphenylphosphine) palladium (0) and copper(I) iodide (CuI) refluxed in a solvent mixture of DMF and triethylamine (Et_3N) at 100 °C for 36 h. After cooling to room temperature, the product was filtered and washed with $6 \text{ mol} \cdot \text{L}^{-1}$ HCl, H_2O and CH_2Cl_2 , respectively, to remove the catalyst and unreacted monomers. Then, the product was further purified by Soxhlet extraction with THF for 36 h. Lastly, the product was dried under vacuum at 100 °C for 8 h to yield yellow powder.

Pore partition of PAFs

Pore partition of PAF-11

PAF-11, PCBP, FeCl_3 and 1,2-dichloroethane were used as raw materials. Under nitrogen atmosphere, after ultrasonication in a 50 mL two-neck round bottom flask for 5 min, the mixture was stirred at 85 °C for 16 h.

The reaction was quenched with MeOH. Then, the mixture was filtered and washed with THF, 6 mol·L⁻¹ HCl, H₂O, and EtOH. Lastly, the product was dried under vacuum at 100 °C for 8 h to yield gray-yellow powder.

Pore partition of PAF-140

PAF-140, PCBP, FeCl₃ and 1,2-dichloroethane were used as raw materials. Under nitrogen atmosphere, after ultrasonication in a 50 mL two-neck round bottom flask for 5 min, the mixture was stirred at 85 °C for 16 h. The reaction was quenched with MeOH. Then, the mixture was filtered and washed with THF, 6 mol·L⁻¹ HCl, H₂O, and EtOH. Lastly, the product was dried under vacuum at 100 °C for 8 h to yield yellow-brown powder.

RESULTS AND DISCUSSION

We employed PAF-11 and PAF-140 as the parent frameworks. The frameworks had plenty of aromatic rings, which provided abundant reacting sites for the pore partition strategy by the Friedel-Crafts reaction. The Friedel-Crafts reaction was used to achieve various degrees of partitioning. The pore spaces of PAF-11 and PAF-140 were partitioned into smaller ones, resulting in several corresponding partitioning PAFs, named PAF-11-px and PAF-140-px, respectively (“p” represents the pore partition agent PCBP) [Figure 1 and Table 1].

The structural features of the resulting PAFs were studied using Fourier transform infrared (FT-IR) and solid-state ¹³C Cross-Polarization and Magic-Angle Spinning Nuclear Magnetic Resonance (CP/MAS NMR). FT-IR spectra of the obtained PAFs were presented in Figure 2A and Supplementary Figures 1-3. The peaks at 3,150-3,450 cm⁻¹ correspond to the stretching vibrations of the -B-OH group of the BDA. The characteristic signals assigned to the -C-Br group of TBPM were located at 504, 534 and 1,077 cm⁻¹ [Supplementary Figure 1]. Compared with TBPM and BDA, the FT-IR spectra of PAF-11 did not reveal the characteristic signals of -B-OH and -C-Br groups, suggesting the consumption of the reactants and the creation of PAF-11. The disappearance of the ≡C-H stretching vibrational peak at 3,265 cm⁻¹ for the corresponding alkynyl monomer and the -C-Br stretching peaks (536, 506 and 1,081 cm⁻¹) for the bromine monomer in Supplementary Figure 2 indicated the complete conversion of the two building units, while the new low-intensity peak observed at 2,207 cm⁻¹ was attributed to the stretching vibration of the -C≡C- in the polymer, which can preliminarily confirm the successful synthesis of PAF-140. As shown in Figure 2A and Supplementary Figure 3, compared with the parent PAFs, the partitioning PAFs showed a clear -CH₂- alkyl stretching vibration peak at 2,910 cm⁻¹ and a complete disappearance of the C-Cl stretching vibration peaks at 678, 725 cm⁻¹, demonstrating the complete Friedel-Crafts reaction and the absence of monomer residues in the PAFs.

Solid-state ¹³C CP/MAS NMR spectroscopy was performed to analyze the chemical environments of carbon atoms in partitioning PAFs. Substituted and unsubstituted aromatic carbon signals were observed in the aromatic carbon region of PAFs, with corresponding chemical shifts of 140 and 127 ppm, respectively [Figure 2B]. The partitioning PAFs exhibited a clear signal peak at 39 ppm, corresponding to the methylene group acquired after the Friedel-Crafts reaction, indicating the successful coupling reaction. Powder X-ray diffraction (PXRD) was performed to study the crystallinity of PAF-11 and corresponding partitioning PAFs, which indicated that the PAFs are amorphous [Supplementary Figure 4]. The morphology of the obtained PAFs was characterized by scanning electron microscopy (SEM). It can be seen from the SEM image that the morphology of PAF-11 presented spherical nanoparticles of 200-300 nm, and the size did not change significantly after pore partition [Supplementary Figure 5]. The same observation was shown for PAF-140 and its corresponding partitioning PAFs, which were essentially spherical nanoparticles of

Table 1. Composition and pore properties of resulting PAFs

Samples	M_{em} (mol) ^a	S_{BET} (m ² ·g ⁻¹) ^b	S_{micro} (m ² ·g ⁻¹) ^c	S_{exter} (m ² ·g ⁻¹) ^d	$R_{Surfacearea}$ (%) ^e	V_{micro} (cm ³ ·g ⁻¹) ^f	$R_{micro\ volume}$ (%) ^g
PAF-11	-	512	268	244	-	0.12	-
PAF-11-p1	0.1	945	514	431	185	0.23	192
PAF-11-p2	0.2	975	569	406	190	0.26	217
PAF-11-p3	0.3	1,042	688	354	204	0.30	250
PAF-11-p4	0.4	1,109	762	347	217	0.33	275

^aRelative to the mole amount of pore partition agent added per 100 mg parent PAF-11. ^bSurface area calculated using the BET equation [Supplementary Figure 7]. ^cMicro pore surface area calculated using t-plot [Supplementary Figure 7]. ^dExternal surface area calculated using t-plot. ^eThe rate of increase in surface area of partitioning PAFs relative to parent PAF-11. ^fMicro pore volume calculated by t-plot. ^gThe rate of increase in micro pore volume of partitioning PAFs relative to parent PAF-11. PAFs: Porous aromatic frameworks; BET: Brunauer-Emmett-Teller.

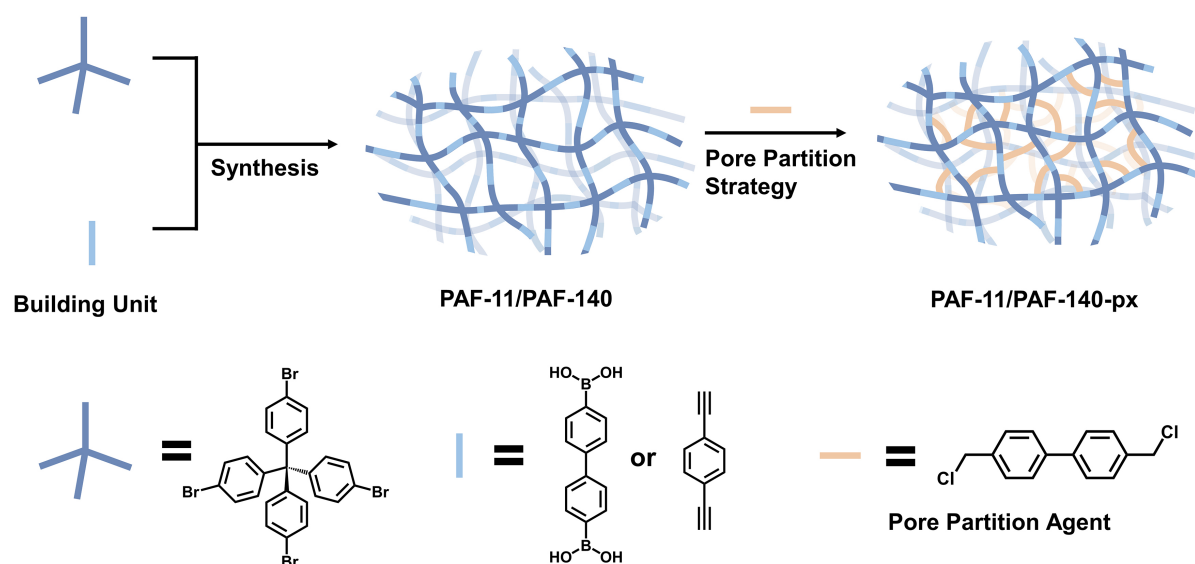


Figure 1. Synthesis route of PAF-11 and PAF-140, and the pore partition strategy to construct extra accessible surface to increase the surface area and segment mesopore into multiple micropore domains. PAF: Porous aromatic framework.

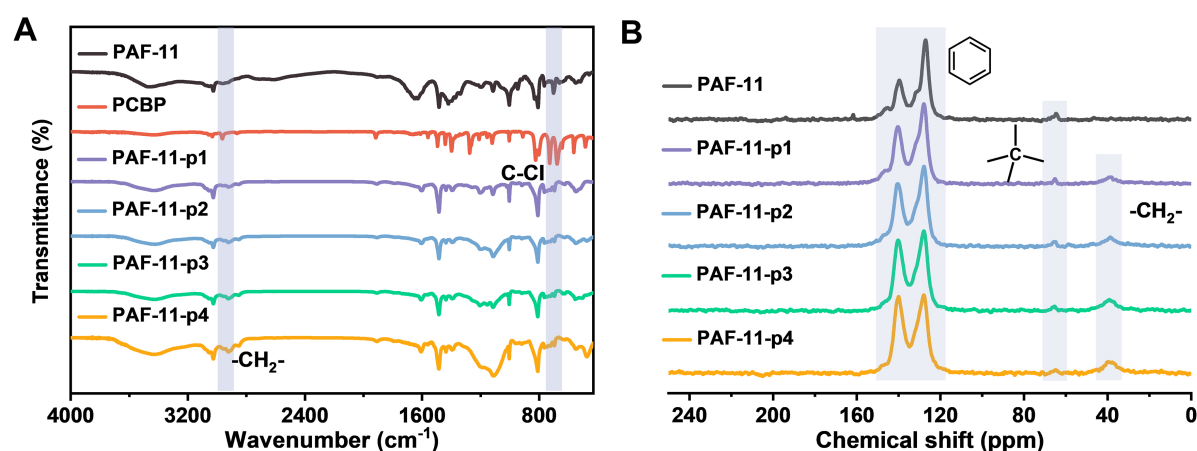


Figure 2. (A) FT-IR spectra of PAF-11 and corresponding partitioning PAFs with different pore partition ratios; (B) Solid-state ¹³C CP/MAS NMR spectrum of PAF-11 and its corresponding partitioning PAFs. FT-IR: Fourier transform infrared; PAF: porous aromatic framework; CP/MAS/NMR: cross-polarization and magic-angle spinning nuclear magnetic resonance.

300–400 nm [Supplementary Figure 6]. These results indicated that the pore partition strategy was a molecular-level modification for the two PAFs without compromising the integrity of their backbones.

As expected, PAFs with high surface areas were successfully synthesized. The porosity of PAFs was investigated by N_2 adsorption analysis at 77 K. It was found that PAF-11 exhibited micro-mesoporous, while all partitioning PAFs exhibited microporous, with a sharp absorption in the low relative pressure region ($P/P_0 < 0.05$), displaying a type-I isotherm [Figure 3A]. When the pressure increased to a higher value ($P/P_0 > 0.9$), a steep absorption occurs, possibly due to the condense of N_2 molecules on the material surface and in the crevices. The Brunauer-Emmett-Teller (BET) model was used to calculate the BET surface area of PAF-11 and its corresponding partitioning PAF, respectively [Supplementary Figure 7]. The surface area (S_{BET}) of PAF-11 was $512 \text{ m}^2\cdot\text{g}^{-1}$, while the S_{BET} of PAF-11-p1, PAF-11-p2, PAF-11-p3 and PAF-11-p4 were up to 945, 975, 1,042 and $1,109 \text{ m}^2\cdot\text{g}^{-1}$, respectively [Figure 3B]. Compared with the parent PAF-11, the surface area of partitioned PAF-11-px increased by 185%, 190%, 204% and 217% [Table 1]. Similarly, the S_{BET} of PAF-140 was calculated to be $705 \text{ m}^2\cdot\text{g}^{-1}$. Compared to the parent PAFs, the S_{BET} of PAF-140-px underwent the similar change. The surface area of partitioning PAF-140-px increased to 915, 960, 992 and $1,067 \text{ m}^2\cdot\text{g}^{-1}$ which were 130%, 134%, 139% and 149% of the parent PAF, respectively [Supplementary Table 1, Supplementary Figures 8 and 9].

Not only did the surface area of the partitioning PAFs increase significantly, but the pore size distribution of PAF-11 and its partitioning PAFs was significantly changed, as indicated by non-local density functional theory (NLDFT) calculations. As shown in Figure 3C, PAF-11 exhibited a wide pore size distribution ranging from 0.7 to 5 nm, including micropores of 1.3 nm, mesopores of 2.3 and 4.1 nm. The pore size of the partitioning PAFs was segmented to create smaller micropore regions, primarily distributed at 0.5 and 1.1 nm. In addition, the micropore volume was also analyzed. Parent PAF-11 exhibited a micropore volume of only $0.12 \text{ cm}^3\cdot\text{g}^{-1}$. The micropore volumes of PAF-11-p1, PAF-11-p2, PAF-11-p3 and PAF-11-p4 were up to 0.23, 0.26, 0.30 and $0.33 \text{ cm}^3\cdot\text{g}^{-1}$, respectively, reaching 192%, 217%, 250% and 275% of the parent framework. Meanwhile, compared to the parent PAF, the micropore surface area of the partitioning PAFs increased while the external surface decreased. According to the results, we concluded that the pore space partition strategy of introducing PCBP with a flexible linkage as a pore partition agent, based on the simple Friedel-Crafts alkylation reaction, was effective for partitioning the rigid PAFs with pure benzene rings. This strategy leads to improvements in surface area, micropore volume and pore size segmentation at the same time. In addition, the surface area of the partitioning PAF-140 increased less than that of the partitioning PAF-11. This difference may be due to the higher benzene ring content in PAF-11 compared to the coexistence of the benzene ring and alkyne bond in PAF-140. This provides more reactive sites for the Friedel-Crafts reaction, leading to a feasible reaction and resulting in a larger increase in surface area. There is less possibility that the pore partition agent will self-polymerize, which is clearly not expected. Thus, the material obtained through self-polymerization reaction of 4,4'-bis (chloromethyl)-1,1'-biphenyl was characterized by N_2 adsorption [Supplementary Figure 10]. The results indicated that the BET surface area of the self-polymer material was calculated to be $985 \text{ m}^2\cdot\text{g}^{-1}$, and the pore size is mainly distributed at 5.3 nm, which is completely opposite to the results of the pore partition strategy. The partitioning PAFs show smaller micropores.

The stability of PAFs is an important factor that influences their practical application. The thermogravimetric analysis (TGA) and chemical stability of the synthesized PAFs were tested. As shown in Supplementary Figures 11 and 12, all the obtained PAFs collapsed at 360 °C. Furthermore, PAF-11 series and two representative PAFs (PAF-11-p4 and PAF-140-p4) were selected for chemical stability testing. It was found that the PAFs did not dissolve or decompose in common organic solvents (such as THF,

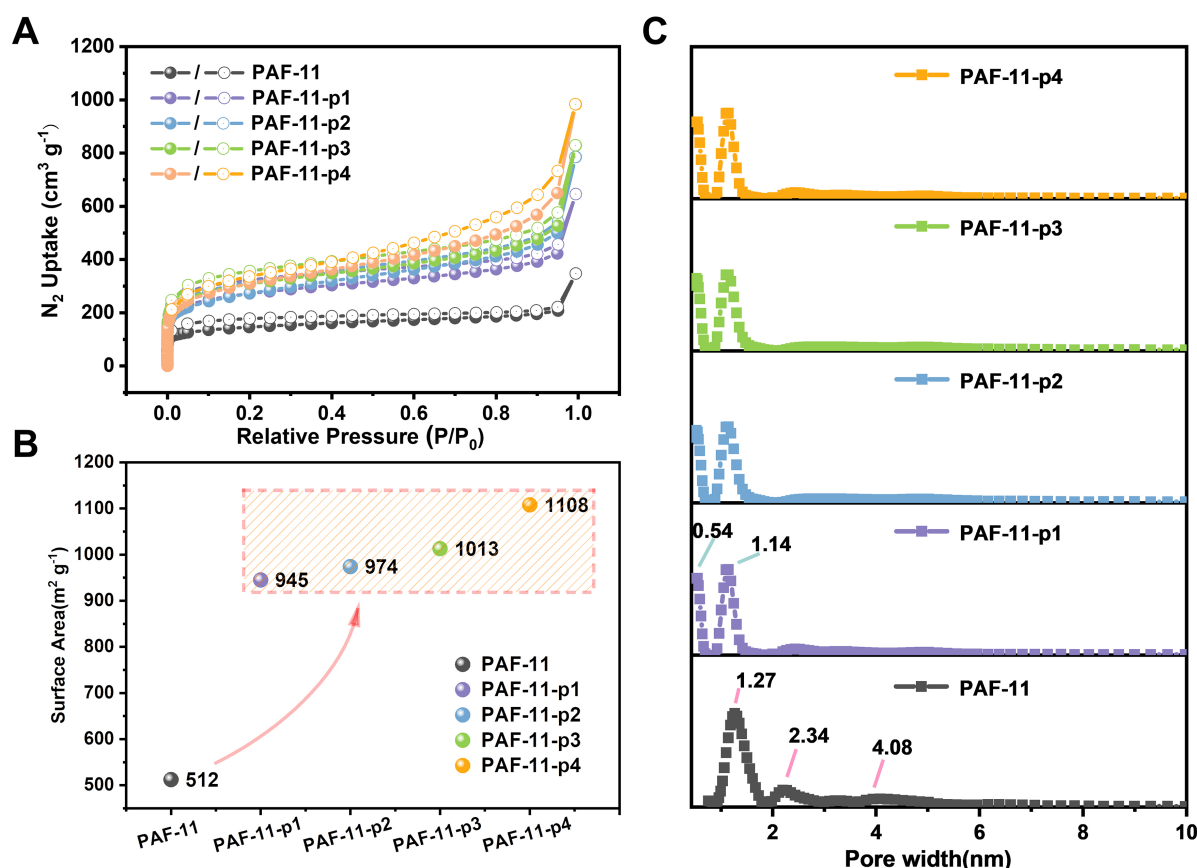


Figure 3. (A) Nitrogen-sorption isotherm curves measured at 77 K of PAF-11 and corresponding partitioning PAFs; (B) Variation range of surface area of PAF-11 and corresponding partitioning PAFs; (C) Pore size distribution changes of PAF-11 and corresponding partitioning PAFs. PAF: Porous aromatic framework.

methanol, dichloromethane, ethanol, acetone, chloroform, DMF, etc.) [Supplementary Figures 13 and 14]. FT-IR and N₂ adsorption experiments showed that the surface area and structure of the as-synthesized materials did not change. The surface area of two PAFs could be kept in the air for over a year at room temperature without significant loss [Supplementary Figure 15]. This demonstrates that PAFs synthesized using the pore partition strategy still exhibit excellent performance.

Given the high surface area, abundant microporosity and excellent stability of partitioning PAFs, their adsorption capacity for CO₂ was explored. The CO₂ adsorption isotherms of PAFs at 273 and 298 K were investigated, respectively. As shown in Figure 4A and B, the CO₂ uptake increased with increasing P/P_0 . At 1 bar, PAF-11, PAF-11-p1, PAF-11-p2, PAF-11-p3 and PAF-11-p4 could adsorb 9.0, 25.7, 25.2, 31.2 and 30.8 cm³·g⁻¹ CO₂ at 298 K, and 18.2, 48.0, 45.6, 51.3 and 54.2 cm³·g⁻¹ CO₂ at 273 K, respectively. The adsorption enthalpy (Q_{st}) of CO₂ adsorption capacities for five PAFs were calculated to be 23.8, 25.9, 25.1, 25.1 and 24.3 kJ·mol⁻¹, respectively [Supplementary Figure 16], showing that the rise of CO₂ adsorption capacity of PAFs was primarily due to the increase of surface area, and PAF-11-p4 exhibiting the highest adsorption capacity of CO₂ among these PAFs.

Due to the significant difference in pore sizes between PAF-11 and its corresponding partitioning PAFs, we conducted adsorption experiments of dye molecules with different sizes. Four anionic and cationic dyes, Acid Blue 93 (AB, anionic), Rhodamine B (RB, cationic), Methyl Blue (MB, cationic) and Methyl Orange

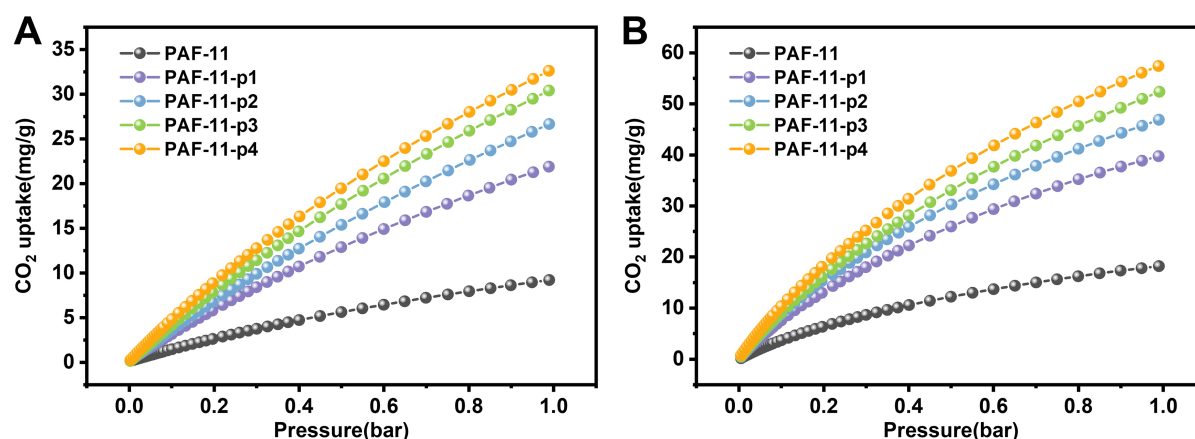


Figure 4. Adsorption isotherms of CO₂ at (A) 298 K and (B) 273 K on PAF-11 and corresponding partitioning PAFs. PAF: Porous aromatic framework.

(MO, anionic), with different molecular sizes, were chosen as the adsorption targets. The nano-sizes of AB, RB, MB and MO were 2.36 nm × 1.74 nm, 1.99 nm × 1.47 nm, 1.88 nm × 0.84 nm, and 1.35 nm × 0.50 nm, respectively. All dyes are polar benzene ring conjugated, which can enhance the adsorption through π - π conjugation with the pure benzene ring system of PAFs. All the adsorption experiments were conducted in aqueous dye solutions at 298 K, with dye concentrations ranging from 20 to 500 mg·L⁻¹ [Supplementary Section 10]. The absorbance of the dye was measured by ultraviolet-visible spectrometry (UV-Vis) and the concentration was calculated by the standard curve [Supplementary Figure 17].

As shown in Figure 5A, the Langmuir isotherm model indicates that PAF-11, despite having a smaller surface area, exhibited the highest maximum uptake (q_{\max}) of 1,488.0 mg·g⁻¹ for large-sized AB. Although the PAF-11-p1, PAF-11-p2, PAF-11-p3 and PAF-11-p4 have a larger surface area, their q_{\max} for AB were 340.0, 362.4, 523.8 and 534.4 mg·g⁻¹, respectively. Furthermore, as shown in Figure 5B and C, the q_{\max} of PAF-11 for RB was 460.8 mg·g⁻¹ according to the Langmuir isotherm model. The q_{\max} of PAF-11-p1, PAF-11-p2, PAF-11-p3 and PAF-11-p4 were 59.1, 115.1, 225.7 and 218.8 mg·g⁻¹, respectively. On the contrary, the q_{\max} of PAF-11 for small-sized MB was 76.5 mg·g⁻¹ according to the Langmuir isotherm model. The q_{\max} of PAF-11-p1, PAF-11-p2, PAF-11-p3 and PAF-11-p4 were 149.3, 283.3, 268.1 and 518.3 mg·g⁻¹, respectively. As shown in Figure 5D, the q_{\max} of PAF-11 for MO was only 57.6 mg·g⁻¹ according to the Langmuir isotherm model. In contrast, the q_{\max} of PAF-11-p1, PAF-11-p2, PAF-11-p3 and PAF-11-p4 were 168.2, 175.7, 203.4 and 218.8 mg·g⁻¹, respectively. The adsorption of PAF-11 and its partitioning PAFs on the four different sizes of dye molecules were better fitted by the Langmuir adsorption model rather than the Freundlich model [Supplementary Figures 18-25]. This suggests that monolayer adsorption was more significant than multilayer physical adsorption. When the pore environment of PAFs was similar, the differences in surface area and pore size were the primary factors contributing to the different adsorption results. When the dye molecule was small enough, the surface area of PAFs dominated the adsorption results, so the adsorption capacity of high surface area partitioning PAFs for small-size MB and MO was much larger than PAF-11. However, PAF-11 exhibited significant adsorption capacity for AB and RB due to its prominent microporosity, which was large enough to accommodate the size of AB and RB. From the discussion and previously reported works^[43-46], it can be seen that the excellent adsorption performance of PAF-11 and its corresponding partitioning PAFs on dye molecules in aqueous solutions is the result of multiple factors. Due to the pure benzene ring structure of the as-synthesized PAFs, they exhibit strong π - π interactions and hydrogen bonding, which dominate the ability of dye adsorption. In addition, the selective adsorption of

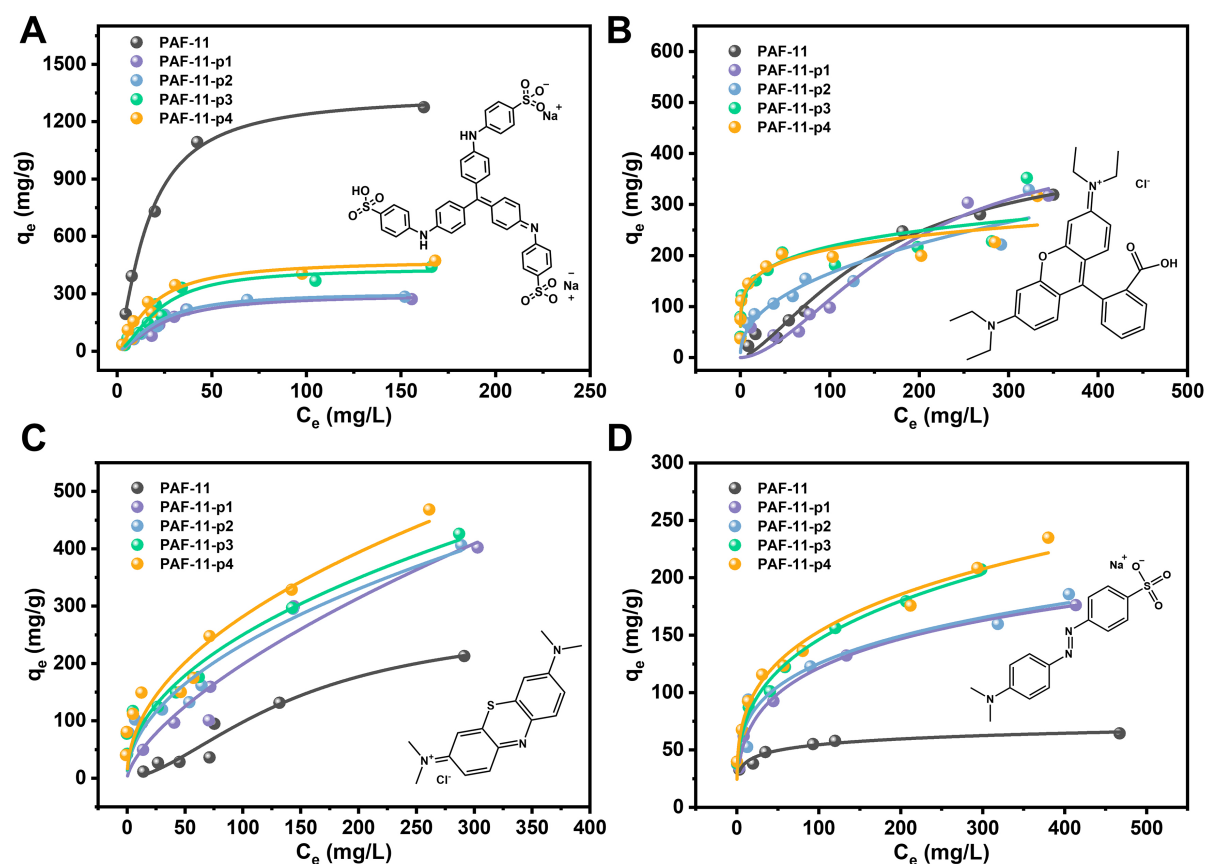


Figure 5. Adsorption of dye molecules (A) AB, (B) RB, (C) MB and (D) MO on PAF-11 and corresponding partitioning PAFs. AB: Acid blue 93; RB: rhodamine B; MB: methyl blue; MO: methyl orange; PAF: porous aromatic framework.

PAFs on dyes with different sizes is clearly dominated by the smaller pore size obtained through the pore partition strategy. Under the synergistic effect of two factors, the parent PAF with a lower surface area has a higher adsorption capacity for large-sized dyes. On the contrary, the partitioning PAFs with higher surface area and microporous pore size have strong adsorption capacity for small-sized dyes.

CONCLUSIONS

In summary, we inserted PCBP with a flexible linkage into PAFs through a Friedel-Crafts alkylation reaction-dominated pore partition strategy, which could provide a straightforward approach for the synthesis of high surface area frameworks while also creating multiple microporous domains. The flexible pore partition agent had a higher pore size tolerance and was more likely to react with the amorphous PAFs. The CO_2 adsorption test showed that the obtained microporous PAFs had a significantly higher CO_2 adsorption capacity compared to the parent PAFs. Dye adsorption experiments revealed that the parent PAFs and partitioning PAFs exhibited diverse adsorption capacities for dye molecules of different sizes, attributed to the segmentation of the pore space. Hence, through this method, the pore partition strategy could be a promising tool to improve the porosity of PAFs in two aspects. This was expected to inspire the creation of diverse libraries of porous solids in various practical applications.

DECLARATIONS

Authors' contributions

Designed the experiments, synthesized samples, carried out characterization, analyzed data, interpreted results, drew the pictures, and wrote the manuscript: Lei H
Conducted material characterization: Zhang Z, Zhai Y, Han X
Analyzed data and contributed helpful discussions: Song J
Revised the manuscript and provided technical support: Li Y
Directed and supervised the project, analyzed data, and revised the manuscript, provided administrative and technical support: Tian Y

Availability of data and materials

Synthetic procedure and results of characterizations can be found in the [Supplementary Materials](#), and the data supporting the findings of this study are available within its [Supplementary Materials](#).

Financial support and sponsorship

The authors are grateful for financial support from the National Natural Science Foundation of China (Grant No. 22075040, No. U21A20330, No. 22131004), the Science and Technology Research project of the Education Department of Jilin Province (JJKH20241414KJ) and Fundamental Research Funds for the Central Universities (2412022QD013).

Conflicts of interest

All authors declared that there are no conflicts of interest.

Ethical approval and consent to participate

Not applicable.

Consent for publication

Not applicable.

Copyright

© The Author(s) 2024.

REFERENCES

1. Barrer RM. Molecular sieve action at low temperatures. *Nature* 1947;159:508. DOI
2. Li Y, Yu J. New stories of zeolite structures: their descriptions, determinations, predictions, and evaluations. *Chem Rev* 2014;114:7268-316. DOI PubMed
3. Wang Q, Astruc D. State of the art and prospects in metal-organic framework (MOF)-based and MOF-derived nanocatalysis. *Chem Rev* 2020;120:1438-511. DOI PubMed
4. Lin JB, Nguyen TTT, Vaidhyanathan R, et al. A scalable metal-organic framework as a durable physisorbent for carbon dioxide capture. *Science* 2021;374:1464-9. DOI PubMed
5. Ding SY, Wang W. Covalent organic frameworks (COFs): from design to applications. *Chem Soc Rev* 2013;42:548-68. DOI PubMed
6. Das S, Heasman P, Ben T, Qiu S. Porous organic materials: strategic design and structure-function correlation. *Chem Rev* 2017;117:1515-63. DOI PubMed
7. Tian Y, Zhu G. Porous aromatic frameworks (PAFs). *Chem Rev* 2020;120:8934-86. DOI PubMed
8. Fan H, Mundstock A, Feldhoff A, et al. Covalent organic framework-covalent organic framework bilayer membranes for highly selective gas separation. *J Am Chem Soc* 2018;140:10094-8. DOI PubMed
9. Ma Y, Cui F, Rong H, et al. Continuous porous aromatic framework membranes with modifiable sites for optimized gas separation. *Angew Chem Int Ed Engl* 2022;61:e202113682. DOI PubMed
10. Li J, Cheng Z, Wang Z, et al. Ultramicroporous covalent organic framework nanosheets with functionality pair for membrane C₂H₂/C₂H₄ separation. *Angew Chem Int Ed Engl* 2023;62:e202216675. DOI PubMed
11. Wang P, Chen X, Jiang Q, et al. High-precision size recognition and separation in synthetic 1D nanochannels. *Angew Chem Int Ed Engl* 2019;58:15922-7. DOI PubMed
12. Yue L, Wang S, Zhou D, Zhang H, Li B, Wu L. Flexible single-layer ionic organic-inorganic frameworks towards precise nano-size

- separation. *Nat Commun* 2016;7:10742. DOI PubMed PMC
13. Lin RB, Li L, Wu H, et al. Optimized separation of acetylene from carbon dioxide and ethylene in a microporous material. *J Am Chem Soc* 2017;139:8022-8. DOI PubMed
 14. Pang JJ, Yao ZQ, Zhang K, et al. Real-time in situ volatile organic compound sensing by a dual-emissive polynuclear Ln-MOF with pronounced Ln^{III} luminescence response. *Angew Chem Int Ed Engl* 2023;62:e202217456. DOI PubMed
 15. Wang Z, Huang Y, Xu K, et al. Natural oxidase-mimicking copper-organic frameworks for targeted identification of ascorbate in sensitive sweat sensing. *Nat Commun* 2023;14:69. DOI PubMed PMC
 16. Lim DW, Sadakiyo M, Kitagawa H. Proton transfer in hydrogen-bonded degenerate systems of water and ammonia in metal-organic frameworks. *Chem Sci* 2019;10:16-33. DOI PubMed PMC
 17. Liu L, Yin L, Cheng D, et al. Surface-mediated construction of an ultrathin free-standing covalent organic framework membrane for efficient proton conduction. *Angew Chem Int Ed Engl* 2021;60:14875-80. DOI PubMed
 18. Song J, Li Y, Cao P, et al. Synergic catalysts of polyoxometalate@cationic porous aromatic frameworks: reciprocal modulation of both capture and conversion materials. *Adv Mater* 2019;31:e1902444. DOI PubMed
 19. Yuan S, Peng J, Cai B, et al. Tunable metal hydroxide-organic frameworks for catalysing oxygen evolution. *Nat Mater* 2022;21:673-80. DOI PubMed
 20. Liu S, Chen H, Zhang X. Bifunctional $\{\text{Pb}_{10}\text{K}_2\}$ -organic framework for high catalytic activity in cycloaddition of CO_2 with epoxides and knoevenagel condensation. *ACS Catal* 2022;12:10373-83. DOI
 21. Li H, Li C, Wang Y, et al. Pore structure unveiling effect to boost lithium-selenium batteries: selenium confined in hierarchically porous carbon derived from aluminum based MOFs. *Chem Synth* 2023;3:30. DOI
 22. Wang L, Wang Y, Li Z, et al. PAF-6 doped with phosphoric acid through alkaline nitrogen atoms boosting high-temperature proton-exchange membranes for high performance of fuel cells. *Adv Mater* 2023;35:e2303535. DOI PubMed
 23. Yuan Y, Zhu G. Porous aromatic frameworks as a platform for multifunctional applications. *ACS Cent Sci* 2019;5:409-18. DOI PubMed PMC
 24. Liu L, Su X, Qi M, Gao X, Ren H, Chen L. Facile synthesis of heteroporous covalent organic frameworks with dual linkages: a “three-in-one” strategy. *Chem Synth* 2024;4:10. DOI
 25. Deng L, Ding Z, Ye X, Jiang D. Covalent organic frameworks: chemistry of pore interface and wall surface perturbation and impact on functions. *Acc Mater Res* 2022;3:879-93. DOI
 26. Lu W, Wei Z, Yuan D, Tian J, Fordham S, Zhou H. Rational design and synthesis of porous polymer networks: toward high surface area. *Chem Mater* 2014;26:4589-97. DOI
 27. Ben T, Ren H, Ma S, et al. Targeted synthesis of a porous aromatic framework with high stability and exceptionally high surface area. *Angew Chem Int Ed Engl* 2009;48:9457-60. DOI PubMed
 28. Zhou DD, Chen P, Wang C, et al. Intermediate-sized molecular sieving of styrene from larger and smaller analogues. *Nat Mater* 2019;18:994-8. DOI PubMed
 29. Zeng H, Xie M, Wang T, et al. Orthogonal-array dynamic molecular sieving of propylene/propane mixtures. *Nature* 2021;595:542-8. DOI PubMed
 30. Dong Q, Huang Y, Wan J, et al. Confining water nanotubes in a $\text{Cu}_{10}\text{O}_{13}$ -based metal-organic framework for propylene/propane separation with record-high selectivity. *J Am Chem Soc* 2023;145:8043-51. DOI PubMed
 31. Lin RB, Li L, Zhou HL, et al. Molecular sieving of ethylene from ethane using a rigid metal-organic framework. *Nat Mater* 2018;17:1128-33. DOI PubMed
 32. Zhai QG, Bu X, Zhao X, Li DS, Feng P. Pore space partition in metal-organic frameworks. *Acc Chem Res* 2017;50:407-17. DOI PubMed
 33. Wei YS, Zhang M, Liao PQ, et al. Coordination templated $[2+2+2]$ cyclotrimerization in a porous coordination framework. *Nat Commun* 2015;6:8348. DOI PubMed PMC
 34. Xiao Y, Chen Y, Hong AN, Bu X, Feng P. Solvent-free Synthesis of multi-module pore-space-partitioned metal-organic frameworks for gas separation. *Angew Chem Int Ed Engl* 2023;62:e202300721. DOI PubMed
 35. Xu X, Wu X, Xu K, Xu H, Chen H, Huang N. Pore partition in two-dimensional covalent organic frameworks. *Nat Commun* 2023;14:3360. DOI PubMed PMC
 36. Hao M, Xie Y, Lei M, et al. Pore space partition synthetic strategy in imine-linked multivariate covalent organic frameworks. *J Am Chem Soc* 2024;146:1904-13. DOI PubMed
 37. Zhang Z, Zheng Y, Dou Z, et al. Multivariate porous aromatic frameworks with high porosity and hierarchical structures for enzyme immobilization. *ACS Cent Sci* 2023;9:488-93. DOI PubMed PMC
 38. Jing Y, Wang C, Chen Y, et al. Crystallinity regulation and defects passivation for efficient and stable perovskite solar cells using fully conjugated porous aromatic frameworks. *Angew Chem Int Ed Engl* 2023;62:e202301234. DOI PubMed
 39. Liu Y, Wang S, Meng X, Ye Y, Song X, Liang Z. Increasing the surface area and CO_2 uptake of conjugated microporous polymers via a post-knitting method. *Mater Chem Front* 2021;5:5319-27. DOI
 40. Jing X, Zou D, Cui P, Ren H, Zhu G. Facile synthesis of cost-effective porous aromatic materials with enhanced carbon dioxide uptake. *J Mater Chem A* 2013;1:13926-31. DOI
 41. Rozyyev V, Thirion D, Ullah R, et al. High-capacity methane storage in flexible alkane-linked porous aromatic network polymers. *Nat Energy* 2019;4:604-11. DOI

42. Yuan Y, Sun F, Ren H, et al. Targeted synthesis of a porous aromatic framework with a high adsorption capacity for organic molecules. *J Mater Chem* 2011;21:13498-502. [DOI](#)
43. Xiao J, Lv W, Xie Z, Tan Y, Song Y, Zheng Q. Environmentally friendly reduced graphene oxide as a broad-spectrum adsorbent for anionic and cationic dyes via π - π interactions. *J Mater Chem A* 2016;4:12126-35. [DOI](#)
44. Hasan Z, Jhung SH. Removal of hazardous organics from water using metal-organic frameworks (MOFs): plausible mechanisms for selective adsorptions. *J Hazard Mater* 2015;283:329-39. [DOI](#) [PubMed](#)
45. Chen T, Zhang W, Li B, et al. Adsorptive separation of aromatic compounds from alkanes by π - π interactions in a carbazole-based conjugated microporous polymer. *ACS Appl Mater Interfaces* 2020;12:56385-92. [DOI](#) [PubMed](#)
46. Durán-jiménez G, Rodríguez J, Stevens L, Kostas ET, Dodds C. Microwave pyrolysis of waste biomass and synthesis of micro-mesoporous activated carbons: the role of textural properties for CO₂ and textile dye adsorption. *Chem Eng J* 2024;488:150926. [DOI](#)